Journal of Nuclear Medicine & Radiation Therapy

Gijs et al., J Nucl Med Radiat Ther 2016, 7:5
DOI: 10.4172/2155-9619.1000300

Research Article Open Access

Biodistribution of Novel ^{68}Ga-Radiolabelled HER2 Aptamers in Mice

Marlies Gijs[1,2], **Guillaume Becker**[2], **Alain Plenevaux**[2], **Mohamed A. Bahri**[2], **An M. Aerts**[1], **Nathalie R.E.N. Impens**[1], **Sarah Baatout**[1] **and André Luxen**[2*]

[1]*Radiobiology Unit, Belgian Nuclear Research Center (SCK•CEN), Mol, Belgium*

[2]*Cyclotron Research Center, University of Liège, Liège, Belgium*

[*]**Corresponding author:** André Luxen, Cyclotron Research Center, Department of Chemistry, University of Liège, Allée du 6 aout 8, 4000 Liège, Belgium, Tel: +32 4 366 23 60; E-mail: aluxen@ulg.ac.be

Recieved date: June 04, 2016; **Accepted date:** August 04, 2016; **Published date:** August 11, 2016

Abstract

Background: Two novel HER2 aptamers were recently selected with great potential for the *in vitro* diagnosis of HER2-positive cancer. The goal of this study was to examine the *in vivo* diagnostic potential of these HER2 aptamers.

Methods: Both HER2 aptamers were radiolabelled with ^{68}Ga, injected in mice bearing a HER2-positive and HER2-negative tumour and evaluated by PET/MRI.

Results: *Ex vivo* bio distribution analysis revealed high uptake in the blood, tissues and organs, except the brain. Interestingly, this high uptake was explained by the slow blood clearance due to non-specific aptamer binding to blood proteins. We observed accumulation of radioactivity in both tumours in time. Although higher uptake in the HER2-positive tumour compared to the HER2-negative tumour was observed, this was accompanied with more necrosis in the HER2-negative tumour, which was observed by ^{18}FDG PET/CT.

Conclusion: This work presents a first step towards the development of ^{68}Ga-labelled aptamers for molecular cancer imaging.

Keywords Aptamers; HER2 receptor; ^{68}Ga; PET imaging; Biodistribution; Tumor-targeting

Introduction

Molecular cancer imaging provides information about all diseased sites in the body (primary tumour and metastases), and avoids biopsy sampling errors due to tumour heterogeneity (within the primary tumor and between the primary tumour and the metastases). It also provides useful targeting and dosimetry information which helps to select the most effective (targeted) cancer therapy regimen. As such, molecular cancer imaging enables the detection, staging, treatment response prediction and treatment follow-up in an accurate and non-invasive way.

One molecular target with high potential for targeted cancer therapy and imaging is the human epidermal growth factor receptor 2 (HER2). HER2 gene amplification and protein overexpression is present in 20% to 25% of all breast cancers, and is associated with poor patient prognosis [1,2]. HER2 has no natural ligands, but monoclonal antibodies and peptides that are able to bind HER2 have been developed. For imaging purposes, full-length antibodies (150 kDa) are less suitable due to slow extravasation and tumour penetration as well as slow clearance of unbound antibody from blood.

Smaller targeting molecules generally provide faster tumour localization and more rapid clearance from blood and healthy tissues, resulting in higher image contrast at early time points after injection. Smaller molecules also can have improved extravasation and increased tumour penetration [3,4]. This was demonstrated by targeting HER2 using antibody fragments (10 kDa to 60 kDa) [5-7] and small proteins (5 kDa to 25 kDa) [8-10].

Aptamers provide a potential alternative to the existing protein-based targeting molecules. Aptamers are small (5 kDa to 15 kDa), non-coding, single-stranded nucleic acid (DNA or RNA) molecules that mimic antibodies in their ability to bind to a specific target. They fold into three-dimensional structures which allow them to bind a specific target with high affinity and specificity. Aptamers possess several advantages over antibodies and proteins such as easy and inexpensive chemical synthesis, low immunogenicity and non-toxicity. Several aptamers targeting HER2 have been reported [11-18]. So far, only one of these aptamers has been radiolabelled (with 99mTc) and its biodistribution was evaluated *ex vivo* [19,20].

The use of smaller molecules with fast pharmacokinetics, such as aptamers, allows radiolabelling with radionuclides with a shorter physical half-life. Regarding diagnostic applications, the use of short-lived radionuclides is beneficial in terms of patient comfort, radiation protection and waste management. In PET imaging, ^{68}Ga is the radionuclide of choice because of its generator availability, easy and stable radiochemistry and appropriate physical half-life (67.71 min).

Although of demonstrated utility in preclinical and limited clinical studies, so far, no ^{68}Ga-radiolabelled pharmaceutical has been approved by the FDA or EMA [21]. However, the market approval of the first ^{68}Ge-^{68}Ga generator in 2014 triggered a new and high interest in the use of ^{68}Ga. Finally, ^{68}Ga is an attractive radionuclide in the view of theranostics, as it can be easily replaced by the therapeutic radionuclides ^{177}Lu or ^{90}Y [22].

Recently, we reported the selection of two novel single-stranded DNA aptamers with high targeting efficacy towards HER2 *in vitro* [23,24]. The goal of this study was to demonstrate the feasibility of these HER2 aptamers for *in vivo* tumour imaging. To this end, we turned both HER2 aptamers into PET imaging agents by radiolabelling them with ^{68}Ga. Subsequently, we evaluated the *ex vivo* biodistribution and tumour targeting properties by PET/MRI imaging.

Materials and Methods

Cell lines and cell culture

Human adherent cancer cell lines MDA-MB-231 (breast adenocarcinoma) and SKOV3 (ovarian adenocarcinoma) were purchased from American Type Cell Culture (ATCC). SKOV3 cells were maintained in McCoy's 5A culture medium (ATCC) supplemented with 20% (v/v) fetal bovine serum (FBS) (Gibco) and incubated in a humidified incubator at 37°C in the presence of 5% CO_2 in air. MDA-MB-231 cells were maintained in Leibovitz's L-15 culture medium (ATCC) supplemented with 10% (v/v) FBS (Gibco) and 100 units/mL, penicillin and 100 µg/mL streptomycin 3232 (Gibco). MDA-MB-231 cells were incubated in a humidified incubator at 37°C in 100% air. All cell lines were dissociated from the culture flask using 5 mM ethylenediaminetetraacetic acid (EDTA, Sigma-Aldrich).

Aptamers

Experiments were performed using the HER2 aptamer HeA2_3 (5'-TCT AAA AGG ATT CTT CCC AAG GGG ATC CAA TTC AAA CAG C-3') or HeA2_1 (5'-ATT AAG AAC CAT CAC TCT TCC AAA TGG ATA TAC GAC TGG G-3') [23]. A negative control aptamer of the same sequence length was also used (5'-CCC TTT TAC ACA ACC ATC GAC ATA ACT AAA ACC ACC ACT G-3'). Aptamer sequences were chemically synthesized by Integrated DNA Technologies (IDT).

Plasma stability assay

The susceptibility to nuclease-mediated degradation of aptamer HeA2_3 was analyzed by a plasma stability assay. In addition, the stability of aptamer HeA2_3 with additional modifications at its terminal ends was evaluated. Aptamer HeA2_3_NOTA was synthesized bearing a hexyldisulfide group at its 5' end. Conjugation to maleimide-NOTA was described as previously reported [24]. Aptamer HeA2_3_NOTA_Inverted T was synthesized with a 5' hexyldisulfide group for conjugation to maleimide-NOTA and a 3' inverted thymidine.

The aptamer samples (1 nmol) were incubated with an equal volume of isolated mouse plasma (obtained in EDTA microtubes according to the manufacturer's protocol, Kent Scientific) and incubated at 37°C for a total of 12 h. At regular time points, aliquots were taken and mixed with equal volumes of stop solution (8 M urea, 50 mM EDTA) and frozen at -20°C. The samples (13.3 pmol aptamer each) were separated on a 15% pre-casted Tris-borate-EDTA (TBE)-Urea polyacrylamide gel (Mini-Protean, Biorad) at 300 V for 60 min. Next, the gels were stained using a 3X GelRed (Biotium) in 0.1 M NaCl post-staining solution and visualized at 254 nm using the Fusion-FX system (Fisher Biotec). Quantification of the bands was performed using Bio-1-D software (Vilber Lourmat). The aptamer half-lives were calculated by fitting the curve to the non-linear one-phase decay model (equation $y=y_0^{-(kx)}$ with y_0=initial band intensity, k=rate constant, half-life=ln2/k) (Graph Pad). All samples were performed in triplicate. Migration of the aptamer bands was compared to migration of the Ultra-Low Range Gene Ruler DNA ladder (Thermo Scientific).

In vivo studies

Animals: Five weeks old female hairless non-obese diabetic severe combined immunodeficient (NOD.Cg-Prkdc^{scid}Hr^{hr}/NCrHsd) mice were purchased from Harlan (Indianapolis, IN, USA). Mice were housed together (3 to 4 mice per cage) in individual ventilated cages and were kept under controlled conditions of 12:12 hour light:dark cycle, 22 ± 2°C and 50 ± 5% relative humidity. The mice were fed ad libitum with irradiated rodent diet (Teklad, Harlan Laboratories) and autoclaved water. The animals were housed at the animal facility of SCK•CEN in accordance with the Ethical Committee Animal Studies of Medanex Clinic (EC_MxCl_2014_034). All animal experiments were done in compliance with the NIH Guides for the Care and Use of Laboratory Animals and were approved by the Ethical Committee of the University of Liège.

Tumour inoculation: Mice were inoculated subcutaneously in the hind leg with a 100 µL cell suspension composed of 50 µL cells in cell culture medium and 50 µL Matrigel basement membrane matrix high concentration (Corning) [25]. MDA-MB-231 cells (3×10^6) were injected into the right flank area at the age of 6 weeks and SKOV3 cells (1.5×10^6) were injected into the left flank area at the age of 7 weeks. Tumour dimensions (largest diameter=a, smallest diameter=b) were measured using a digital calliper (VWR) and calculated using the following equation: volume (mm^3)=$a \times b^2 \times 0.5$. Tumour volume and animal weight were carefully monitored two to three times per week.

Aptamer radiolabelling: Radiolabelling was performed as described before [26]. Briefly, the aptamer was functionalized with a disulfide group and conjugated to MMA-NOTA. HPLC and ESI-MS analyses indicated successful conjugation. ^{68}Ga was eluted from a ^{68}Ge-^{68}Ga generator (IRE-Elit) using 1.2 mL 0.1 N HCl, purified using 100 mg strong-cation exchange Chromabond cartridges (Machery-Nagel), and subsequently eluted with 250 µL 5 M NaCl (in 0.1 N HCl). Radiolabelling was performed using 2.5 nmol lyophilized aptamer in 300 µL HEPES buffer (pH 4.4). A 100 µL fraction ^{68}Ga was added to the aptamer and incubated for at least 5 min at room temperature. Radio-TLC analysis confirmed quantitative radiolabelling.

Small-animal PET imaging: Small-animal PET imaging was performed on a Siemens Concorde Focus 120 microPET (Siemens). To correct for attenuation, a 10 min transmission scan using a ^{57}Co point source and an energy window of 120 keV to 125 keV was performed. Each animal was placed in a dedicated mice holder allowing for regulated temperature control and anaesthesia delivery. Anaesthesia was induced with 4% isoflurane in oxygen and maintained by inhalation of 1% to 2% isoflurane. After PET imaging, structural images for co-registration and segmentation were acquired with a micro-CT scanner (eXplore 120, TriFoil) or 9.4 Tesla micro-MRI (Agilent).

Tumour imaging with ^{18}FDG: Each mouse was scanned with 2-deoxy-2-[^{18}F] fluoro-D-glucose (^{18}FDG) maximum one week before imaging with the ^{68}Ga-radiolabelled HER2 aptamers. Mice were fasted overnight with free access to water. The animals were warmed (30°C to 34°C) for 30 min before the acquisition and throughout the uptake and imaging period in order to reduce tracer uptake in fat brown tissue. A solution of 10 MBq ^{18}FDG was injected intraperitoneally. A 10 min static PET scan was performed 60 min p.i. Subsequently, mice were scanned by CT. Following image reconstruction, microPET and CT

images were manually co-registered using the commercially available research software π.PMOD (version 3.6, PMOD Technologies) [27,28].

Tumour imaging with ^{68}Ga-radiolabelled HER2 aptamers: Mice were injected in the tail-vein with the ^{68}Ga-radiolabelled HER2 aptamer HeA2_3 (n=6), HeA2_1 (n=9) or negative control aptamer (n=6). Injections were performed using a 10 MBq solution of ^{68}Ga-radiolabelled HER2 aptamer. Unlabelled aptamer was added to the solution to reach a total of 1 nmol aptamer. Dynamic scanning was performed for 60 min immediately post injection (p.i.). Subsequently, mice were scanned by MRI. Following image reconstruction, microPET and MRI images were manually co-registered using the commercially available research software π.PMOD (version 3.6, PMOD Technologies).

PET Quantitative Analysis of ^{68}Ga-radiolabelled aptamer concentration: Quantitation was performed with π.PMOD (version 3.6, PMOD Technologies). To quantify radioactivity within the tumours and main organs, regions-of-interest (ROIs) were manually drawn in representative organ data spaces relative to visual anatomic landmarks. Standardised uptake values (SUVs) were calculated by dividing the tracer activity per unit mass by the amount of injected activity per unit body mass, assuming a density of 1 g/cm^3.

Ex vivo **biodistribution of the ^{68}Ga-radiolabelled aptamer:** Organ and tumour harvesting was performed 105.4 ± 11.7 min p.i. of the ^{68}Ga-radiolabelled HER2 aptamers. The tissues were weighed (NewClassic ML, Mettles Toledo) and counted for radioactivity using a gamma well counter (Cobra II Auto-Gamma, Perkin-Elmer). All measurements were decay-corrected and normalized to the total injected activity. The tissue radioactivity was expressed as a mean ± SD % injected dose (ID)/g tissue. These data were further used to calculate tumour-to-background ratios. Significant differences were evaluated by two-way ANOVA (Graphpad).

Blood perfusion assay: A blood perfusion assay was performed 90 min p.i. of the ^{68}Ga-radiolabelled aptamer in non-tumour bearing NOD.Cg-Prkdc^{scid}Hr^{hr}/NCrHsd mouse. The mouse was anaesthetized with sodium pentobarbital (Nembutal) and injected intracardially with heparin solution (25 units per mL of 0.9% NaCl). Next, the mouse was perfused with PBS into the left ventricle for 3 min at 12 mL/min using a syringe pump. Afterward, the mouse was dissected and the main organs were harvested and measured for radioactivity as described above.

Blood collection: Whole blood was collected in Microtainer Blood Collection Tubes containing Lithium Heparin/ PST Gel (Becton Dickinson). Next, the tube was centrifuged for 2 min at 6,800 rpm (Bioblock Scientific, Sigma 2-15 centrifuge) to separate the plasma from the blood cells. For protein precipitation, an equal volume of 100% acetonitrile was added to the plasma to separate the serum from the blood proteins. The solution was vortexed and centrifuged for 2 min at 25,000 rpm (Avanti 30 centrifuge, Analis). The amount of radioactivity in the whole blood, plasma, blood cells, serum and blood proteins was measured using a gamma well counter (Cobra II Auto-Gamma, Perkin-Elmer).

Results and Discussion

Plasma stability of aptamer HeA2_3

In vivo applications of aptamers require that they remain stable in physiological conditions for a substantial amount of time. In general, DNA oligonucleotides are susceptible to nuclease-mediated degradation *in vivo* with a half-life varying from 30 min to 60 min [29]. In order to avoid 5' and 3' exonuclease activity, aptamers can be chemically modified at their terminal ends. We evaluated the *in vitro* stability of aptamer HeA2_3 bearing a 5' NOTA modification or a 5' NOTA modification combined with a 3' inverted thymidine (T) modification. After 12 h of incubation in isolated mouse plasma, the samples were analysed by denaturing PAGE gel electrophoresis. The results were quantified (Bio-1-D software) and the biological half-life was estimated by fitting the data using a non-linear one-phase decay model.

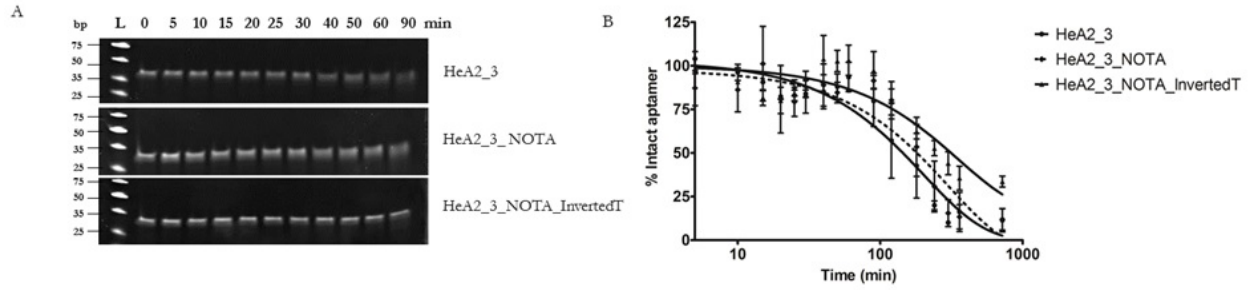

Figure 1: (A) Separation of the aptamer samples by denaturing PAGE gel electrophoresis following incubation (0 min to 720 min) in isolated mouse plasma at 37°C. The samples which were incubated from 0 min to 90 min are presented (B) The mean ± SEM% intact aptamer (relative to time point 0) was plotted as a function of the incubation time (log min) (0 min to 720 min) and fitted using a non-linear one-phase decay model (GraphPad). Significance was tested by Two-way ANOVA. No significance was observed.

As shown in Figure 1A, the intensity of the band (representing the amount of intact aptamer) decreases with time, indicating degradation of the full-length product (40-mer). The biological half-life of the unmodified aptamer was about two hours (121.9 min ± 45.1 min) (Figure 1B). Protecting the 5' end by conjugation to maleimide-NOTA considerably improved the biological half-life (162.1 min ± 57.1 min). Finally, addition of an extra 3' terminal cap (inverted T) to the 5' NOTA-conjugated aptamer further increased stability (biological half-life of 184.6 min ± 21.5 min). These findings indicate that protection of the 5' and 3' ends by functional or chemical groups considerably

improves the aptamer stability against nuclease-mediated degradation in mouse plasma, and therefore makes the aptamer suitable for *in vivo* use. We continued our study with the 5' NOTA conjugated aptamer (without inverted T), since the biological half-life is sufficiently for ^{68}Ga studies (physical half-life=68 min) and since the addition of more modifications may change the aptamer structure, binding capacity and function. The NOTA chelator will be used for complexation of ^{68}Ga (see further).

Mouse model

We developed a mouse model bearing a different tumour (i.e. one HER2-positive and one HER2-negative tumour) at each flank. This approach provides an ideal negative control and enables easy comparison between the two tumours. In addition, it allows reducing the total amount of animals. We used the recently developed hairless NOD.SCID mouse model (NOD.Cg-Prkdc^{scid}Hr^{hr}/NCrHsd mouse, or commonly named SCID hairless NOD (SHrN™, Harlan Laboratories)) [30,31]. This mouse model is ideal for tumour xenografting because the mice are triple-immunodeficient and hairless (enabling easy visual inspection of subcutaneous tumour xenografts).

A pilot study was performed to evaluate tumour growth of several HER2-positive and HER2-negative cell lines. Mice were injected subcutaneously with various concentrations of SKOV3, SKBR3 or MDA-MB-231 cells in Matrigel.

Tumour growth was externally measured using a digital calliper. Although xenografting of SKBR3 cells has been established previously in other mouse models [32-34], no tumour growth of the SKRB3 xenografts could be observed in the SCID hairless NOD mice. We noticed faster tumour growth for the SKOV3 xenografts versus the MDA-MB-231 xenografts (data not shown).

Therefore, we decided to inject a higher number of MDA-MB-231 cells (3×10^6 cells) and at an earlier time point than the SKOV3 cells (1.5×10^6 cells). Figure 2 shows the experimental set-up, including tumour cell injections, ^{18}F-FDG PET/CT scan and ^{68}Ga-radiolabelled HER2 aptamer PET/MRI scan. All mice were analysed at the same age.

Tissue biodistribution

The tissue biodistribution of the ^{68}Ga-radiolabelled HER2 aptamers HeA2_3, HeA2_1 and a negative control aptamer was examined in tumour-bearing mice. All three aptamers showed relatively high uptake in the main organs, except the brain (Figure 3).

The lower uptake in the brain may reflect no access of the ^{68}Ga-radiolabelled HER2 aptamer to the brain because of the blood-brain barrier (BBB). This result is in accordance with previous studies which showed that aptamers are not able to cross the BBB passively [35-37].

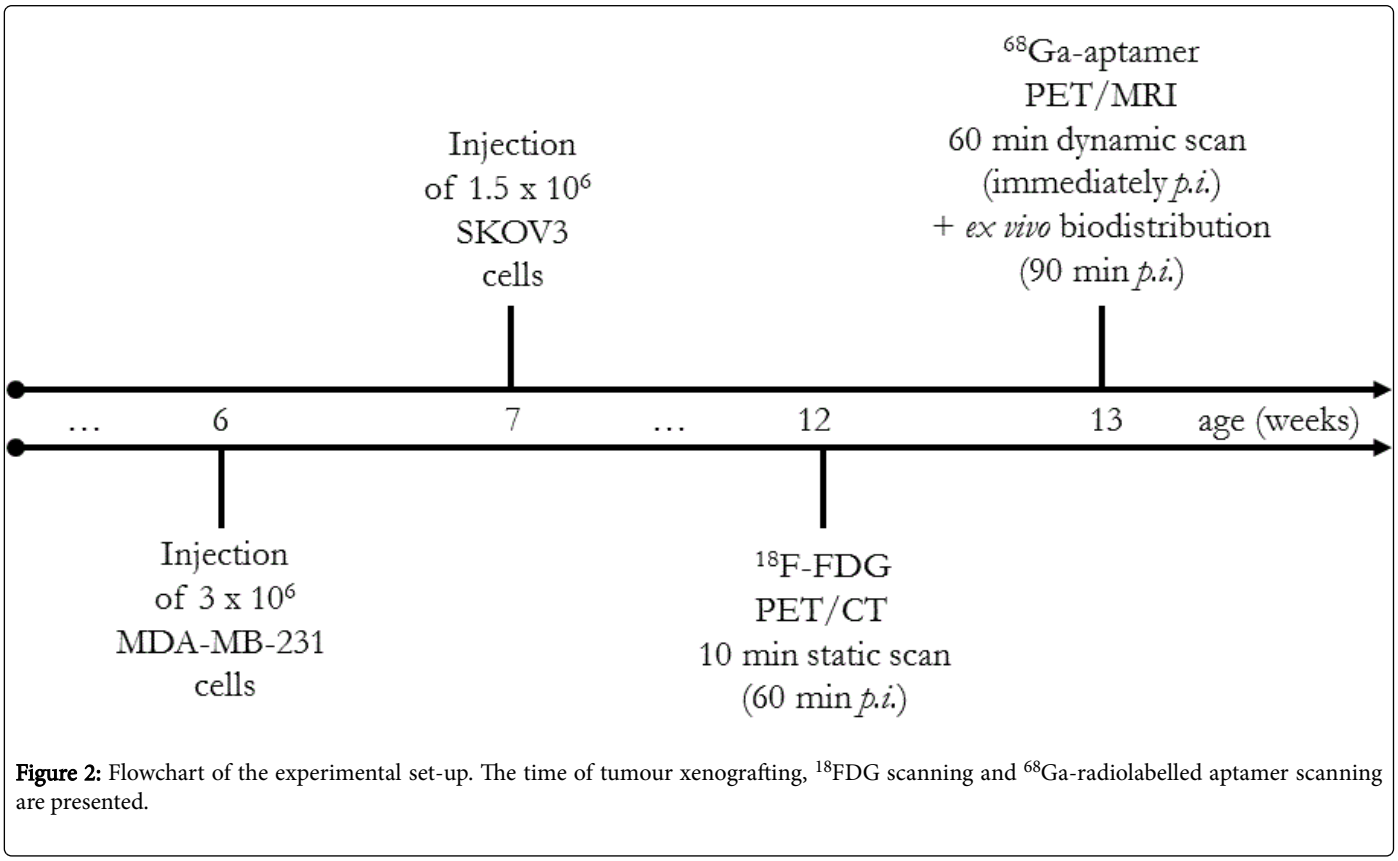

Figure 2: Flowchart of the experimental set-up. The time of tumour xenografting, ^{18}FDG scanning and ^{68}Ga-radiolabelled aptamer scanning are presented.

There were no significant differences between the two HER2 aptamers and the negative control aptamer, except a significant increase in kidney uptake for the negative control aptamer, which may be related to the difference in nucleotide sequence and therefore difference in hydrophilicity.

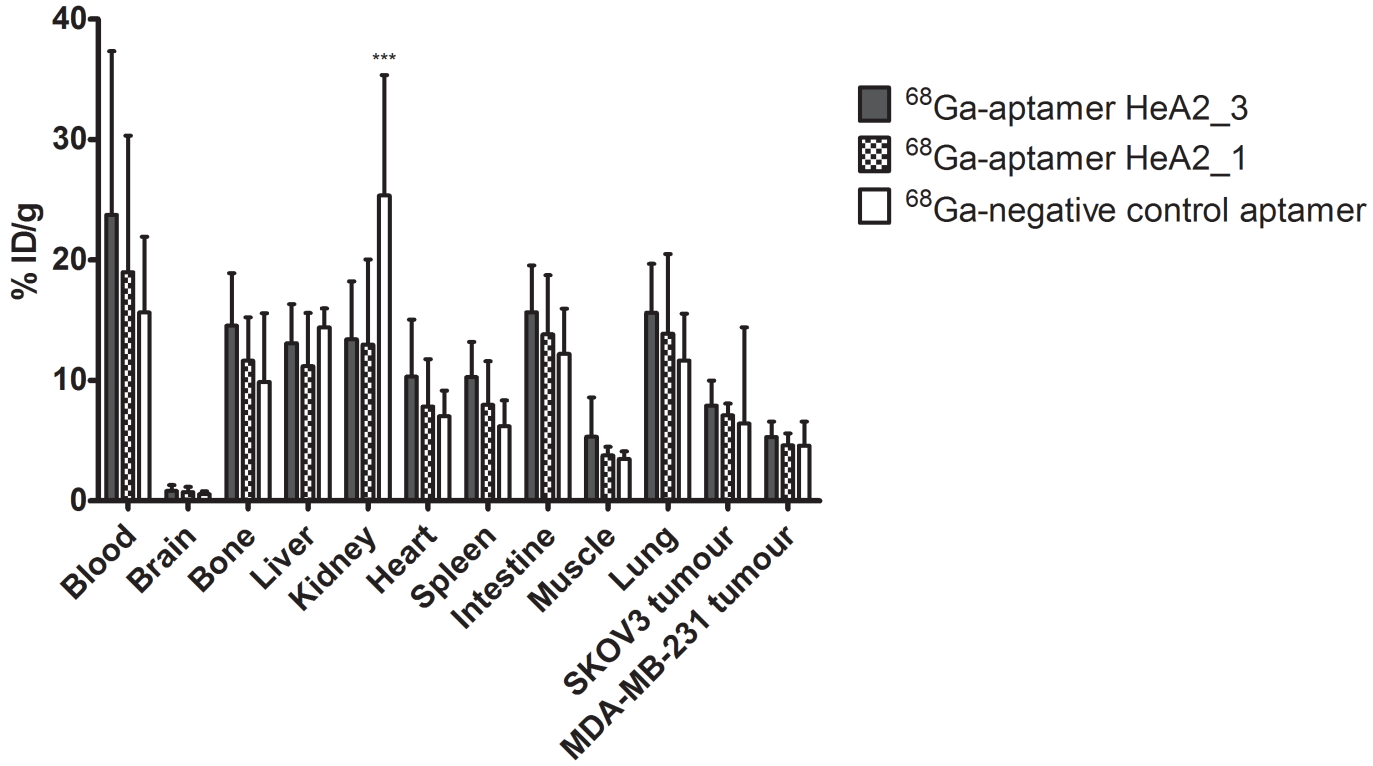

Figure 3: *Ex vivo* tissue biodistribution in tumour-xenografted mice. Analysis at 105.4 ± 11.7 min p.i., data are expressed as mean ± SD% ID/g, n=9 (aptamer HeA2_1) and n=6 (aptamer HeA2_3 and negative control aptamer). Significant differences between the three aptamers per organ or tissue was tested by Two-way ANOVA, $p<0.001$ (***).

The high uptake in the main organs may correspond to the presence of radioactivity in the blood in these organs. Therefore, we performed a blood perfusion assay using non-tumour bearing mice in order to wash out the blood in the organs. As such, it gives an idea about the actual tissue uptake in the main organs, which may be masked by the presence of the radioactivity in the blood.

Figure 4A confirms that the main uptake in the organs was due to the presence of the radioactivity in the blood. Figure 4A also reveals low uptake in all organs after blood perfusion, which indicates low non-specific binding to the tissue.

This suggests that aptamers may be advantageous to proteinous imaging agents, which often have high non-specific uptake in the kidneys (e.g. nanobodies) [38] and intestine (e.g. nanofittins) (own observations). We did not observe bone accumulation after blood perfusion which also confirms the stability of the radiolabelled complex, since free ^{68}Ga is known to accumulate in the bone when released from the chelator [39].

In order to analyse the radioactivity in the blood in more detail, we separated the whole blood into plasma, blood cells, serum and blood proteins, and analysed the radioactivity in each fraction. Figure 4B shows that the entire (100%) radioactivity in the whole blood (expressed as % ID/g) was present in the plasma, of which 17.3% remained present in the serum. As such, the radioactivity in the blood was mainly present on the blood proteins.

The biological half-life of the (unlabelled) aptamer in plasma is 162.1 min ± 57.1 min (Figure 1B). As such, we expected that about one fourth of the injected aptamers is metabolised after 90 min. Therefore, a part of the observed radioactivity in the blood may originate from radioactive metabolites.

We previously showed *in vitro* that no transchelation of ^{68}Ga from the ^{68}Ga-radiolabelled aptamers to transferrin or serum proteins occurred [26]. Therefore, the high radioactivity in the blood proteins may be explained by non-specific aptamer binding to blood proteins such as the highly abundant albumins and globulins. These blood proteins are well-known to bind oligonucleotides in a non-specific manner [40-42].

The same behaviour has also been observed for a variety of drugs, such as aspirin [43,44]. Pre- or co-infusion with a non-targeting aptamer may be used to saturate blood proteins. Another reason for the high radioactivity in the blood may be the (specific) binding of the

aptamer to soluble HER2 protein in blood circulation. The presence of soluble HER2 has been observed in approximately 18% of HER2-positive cancer patients, and is caused by shedding of the extracellular domain of the membrane-bound HER2 receptor [45,46].

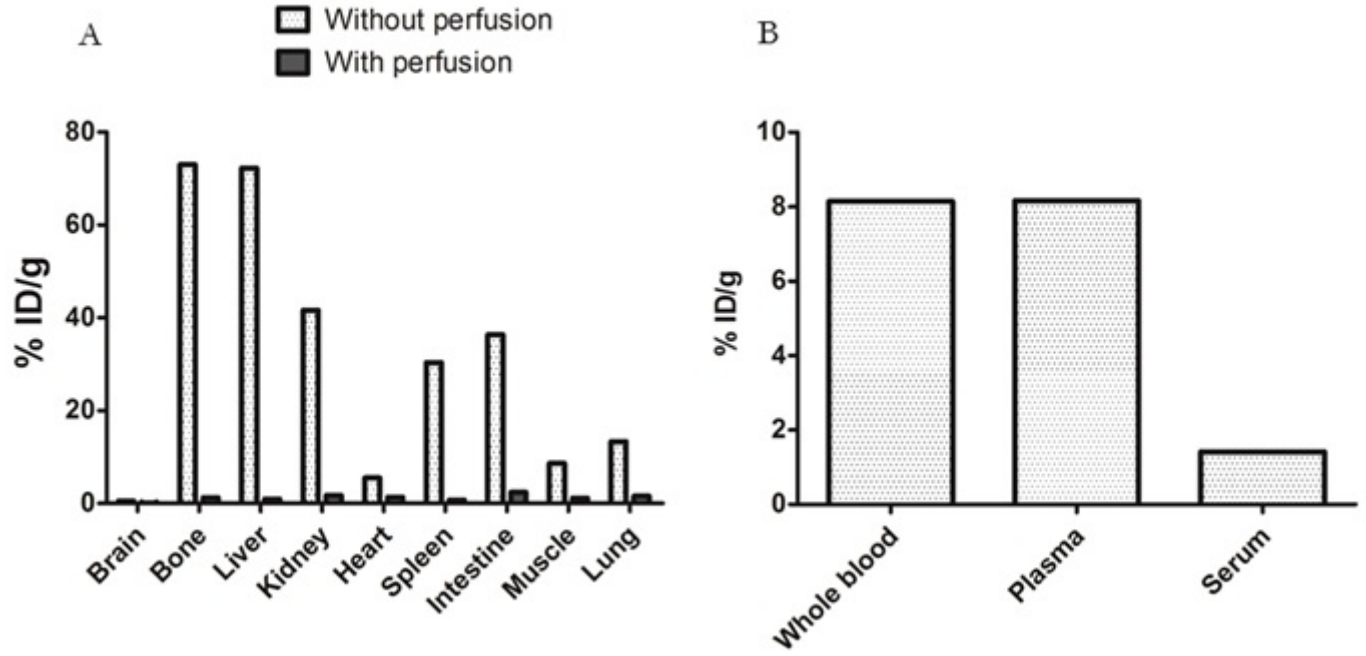

Figure 4: (A) *Ex vivo* tissue biodistribution in non-tumour-xenografted mice with and without perfusion. (B) Analysis of the radioactivity in different blood fractions. Analysis 90 min p.i. of the ^{68}Ga-radiolabelled negative control aptamer, data are expressed as mean % ID/g tissue, n= 1.

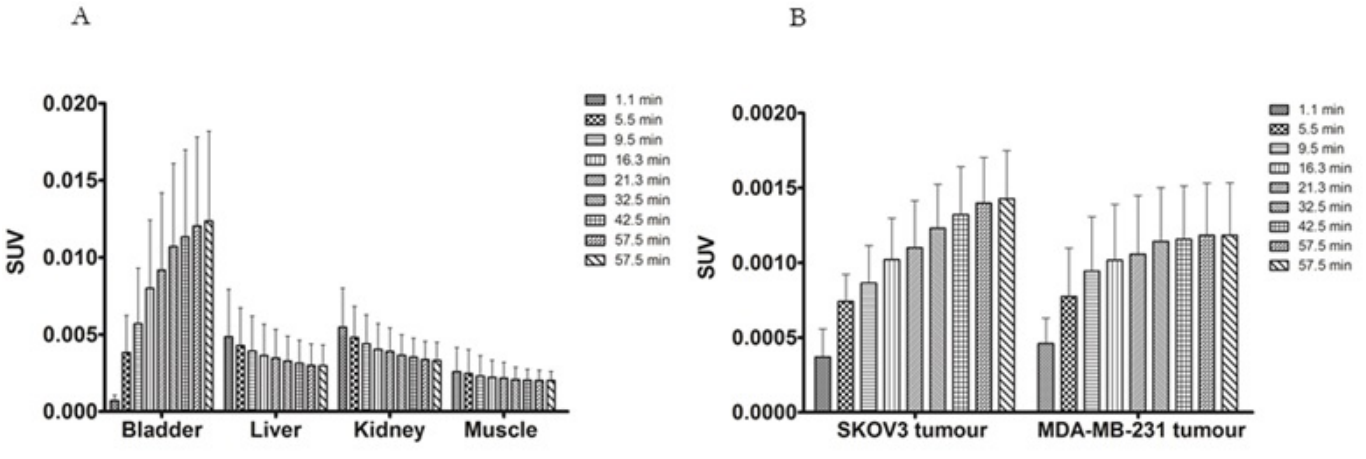

Figure 5: ^{18}FDG analysis of tumour metabolic activity by PET/CT static scanning. The mouse bears the MDA-MB-231 tumour at the right flank and the SKOV3 tumour at the left flank.

Tumour uptake

Ex vivo biodistribution revealed high uptake for both ^{68}Ga-radiolabelled HER2 aptamers in the SKOV3 tumour (7.9 ± 2.1% ID/g for aptamer HeA2_3 and 7.1 ± 1% ID/g for aptamer HeA2_1) (Figure 3). In addition, both ^{68}Ga-radiolabelled HER2 aptamers show a 1.5-fold higher uptake in HER2-positive tumour (SKOV3 tumour) versus the HER2-negative tumour (MDA-MB-231 tumour).

However, the same behaviour was observed for the negative control aptamer and no significant differences in SKOV3 tumour uptake could be observed between the HER2 aptamers (HeA2_1 and HeA2_3) and

the negative control aptamer. These results suggest that tumour uptake was more related to the tumour composition factors (such as cellular composition, EC matrix, vascular network, lymphatic system and necrosis) than to the expression of HER2.

^{18}FDG PET scanning revealed heterogeneous ^{18}FDG uptake due to tumour necrosis. We observed more often necrotic centres in the MDA-MB-231 tumours versus SKOV3 tumours. This may explain the lower uptake of the ^{68}Ga-radiolabelled aptamers in the MDA-MB-231 tumours. These results also demonstrate the importance of analysing the xenografted tumours by ^{18}FDG PET.

We evaluated the kinetic behaviour of the ^{68}Ga-radiolabelled aptamers using dynamic PET scanning. Regions of interest were drawn on the bladder, liver, kidney, paravertebral muscle and on both tumours. Analysis of the heart region was not possible because this was located out of the imaging field. At multiple selected time points, the data were extracted from time-activity curves and the SUV values were calculated. Figure 5 shows the SUV values of ^{68}Ga-radiolabelled aptamer HeA2_1. Aptamer HeA2_3 and negative control aptamer had a similar behaviour.

Figure 5A shows rapid tissue (liver and kidney) accumulation and gradual release, reflecting renal and hepatobiliary clearance. Accumulation in the bladder also indicates renal clearance. While the radioactivity in the main tissues (liver, kidney and muscle) decreases in time (Figure 5A), we observed rapid tumour uptake which slowly continued to increase in time (Figure 5B).

We hypothesize that the long residence time of the ^{68}Ga-radiolabelled aptamers in the blood (as described above) leads to this accumulation in tumour tissue. This also suggests that the affinity of the ^{68}Ga-radiolabelled aptamers for the tumour tissue is higher than for the blood proteins.

In contrast to the SKOV3 tumour, the MDA-MB-231 tumour seemed to have reached a maximum uptake after 32.5 min. This suggests saturation of (non-specific) receptors and binding sites in the tumour tissue. The persistent increase of accumulation in the SKOV3 tumour may reflect additional (specific) HER2 binding. Further investigation using later time points of analysis are needed in order to evaluate this. An increasing accumulation of radiolabelled aptamer in time (up to 5 h p.i.) has been often observed with other aptamers [19,20,47-49].

From these experiments, it is not possible to evaluate (specific) tumour binding capacity of the ^{68}Ga-radiolabelled aptamers, since this may be masked by the high (non-specific) binding to blood proteins. We previously confirmed the HER2 expression level of both tumours, as well as specific binding of (fluorescently labelled) HER2 aptamers to HER2-positive tumour tissue sections [24]. However, these *in vitro* experiments were performed in the absence of blood proteins. Therefore, a blood perfusion assay on tumour-bearing mice is recommended to confirm specific binding of the ^{68}Ga-radiolabelled aptamers to the tumour xenografts *in vivo*.

Conclusion

The goal of this study was to evaluate the general biodistribution profile of two novel HER2 aptamers and to demonstrate the feasibility of these ^{68}Ga-radiolabelled HER2 aptamers for imaging of HER2-positive tumours. *Ex vivo* biodistribution analysis of the ^{68}Ga-radiolabelled aptamers revealed high uptake in the blood, tissues and organs, except the brain. Preliminary results from a blood perfusion assay suggested that the uptake in the tissues and organs was due to the presence of radioactivity in the blood. Analysis of the radioactivity in the different blood fractions showed that the major part of radioactivity was present in the blood proteins. In contrast to the rapid uptake and gradual release of radioactivity in the kidney, liver and muscle, we observed accumulation of radioactivity in both tumours in time. However, no significant differences between both tumour types and between the HER2 aptamers and the negative control aptamer could be observed.

The slow clearance from the blood stream may be an issue regarding the signal-to-noise ratio and the overall quality of PET images, but may be good for tumour targeting. The main future challenge of aptamers (and oligonucleotides in general) is mastering the non-specific interactions *in vivo* [41,50]. Non-specific interactions are certainly the major pitfall for specific imaging of biological targets with aptamers, as it results in a high background noise and therefore low image contrast. In addition, high specificity is important to avoid false-positive diagnoses. For therapy, the concentration of aptamer at the target site is much more important than the signal-to-noise ratio. Therefore, non-specific interactions are less crucial for therapeutic applications, as long as it doesn't lead to adverse side effects.

References

1. Slamon DJ, Clark GM, Wong SG, Levin WJ, Ullrich A, et al. (1987) Human breast cancer: correlation of relapse and survival with amplification of the HER-2/neu oncogene. Science 4785: 177-182.
2. Slamon DJ (1984) Studies of the HER-2/neu proto-oncogene in human breast and ovarian cancer. Science 4905: 707-712.
3. Orlova A, Magnusson M, Eriksson TL, Nilsson M, Larsson B, et al. (2006) Tumor imaging using a picomolar affinity HER2 binding affibody molecule. Cancer Res 8: 4339-4348.
4. Xiang D, Zheng C, Zhou SZ, Kong L, Liu K, et al. (2015) Superior Performance of Aptamer in Tumor Penetration over Antibody: Implication of Aptamer-Based Theranostics in Solid Tumors. Theranostics 10: 1083-1097.
5. Carrasquillo J (2013) Biodistribution and Dosimetry of Serial PET Imaging With Ga-68 Labeled F(ab') 2- Trastuzumab.
6. Ueda M, Hisada H, Teema T, Shimizu Y, Kimura H, et al. (2015) Gallium-68-labeled anti-HER2 single-chain Fv fragment: development and in vivo monitoring of HER2 expression. Mol Imaging Biol 1: 102-110.
7. Keyaerts M, Xavier C, Heemskerk J, Deevoogdt N, Everaert H, et al. (2014) First-in-human Study of ^{68}GaNOTA-Anti-HER2 Nanobody, a New Radiopharmaceutical for Positron Emission Tomography (PET) Imaging of HER2 Expression in Breast Carcinoma Patients. WMIC Scientific Session 01: SS 1.
8. Baum RP, Prasad V, Muller D, Orlova A, Wennborg A, et al. (2010) Molecular imaging of HER2-expressing malignant tumors in breast cancer patients using synthetic 111In-or ^{68}Ga-labeled affibody molecules. J Nucl Med 6: 892-897.
9. Lindman H (2015) PET Study of Breast Cancer Patients Using [68Ga]ABY-025.
10. Ren G, Zhang R, Liu Z, Webster JM, Miao Z, et al. (2009) A 2-helix small protein labeled with ^{68}Ga for PET imaging of HER2 expression. J Nucl Med 9: 1492-1499.
11. Kim MY, Jeong S (2011) In vitro selection of RNA aptamer and specific targeting of ErbB2 in breast cancer cells. Nucleic Acid Ther 21: 173-178.
12. Kang HS, Min YH, Youn SK, Ki DL (2009) Isolation of RNA Aptamers Targeting HER-2-overexpressing Breast Cancer Cells Using Cell-SELEX. Bull Korean Chem Soc 8: 1827-1831.
13. Thiel KW (2012) Delivery of chemo-sensitizing siRNAs to HER2+-breast cancer cells using RNA aptamers. Nucleic Acids Res 40: 6319-6337.

14. Mahlknecht G, Maron R, Mancini M, Schechter B, Sela M, et al. (2013) Aptamer to ErbB-2/HER2 enhances degradation of the target and inhibits tumorigenic growth. Proc Natl Acad Sci USA 20: 8170-8175.
15. Gupta S (2011) Rapid histochemistry using slow off-rate modified aptamers with anionic competition. Appl Immunohistochem Mol Morphol 3: 273-278.
16. Dastjerdi K, Tabar GH, Dehghani H, Haghparast A (2011) Generation of an enriched pool of DNA aptamers for an HER2-overexpressing cell line selected by Cell SELEX. Biotechnol Appl Biochem 58: 226-230.
17. Hu Y, Duan J, Cao B, Zhang L, Lu X, et al. (2015) Selection of a novel DNA thioaptamer against HER2 structure. Clin Transl Oncol 1-10.
18. Liu Z, Duan JH, Song YM, Ma J, Wang FD, et al. (2012) Novel HER2 Aptamer Selectively Delivers Cytotoxic Drug to HER2-positive Breast Cancer Cells in vitro. J Transl Med 1: 148.
19. Varmira K, Hosseinimehr SJ, Noaparast Z, Abedi SM (2013) A HER2-targeted RNA aptamer molecule labeled with 99mTc for single-photon imaging in malignant tumors. Nucl Med Biol 8: 980-986.
20. Varmira K, Hosseinimehr SJ, Noaparast Z, Abedi SM (2014) An improved radiolabelled RNA aptamer molecule for HER2 imaging in cancers. J Drug Target 2: 116-122.
21. Banerjee SR, Pomper MG (2013) Clinical applications of Gallium-68. Appl Radiat Isot 76: 2-13.
22. Baum R, Rösch F (2013) Theranostics, gallium-68 and other radionuclides. Springer.
23. Penner G (2015) US 2015/62182945 A1. N.B. Inc., Clyde, Alberta, Canada.
24. Gijs M, Penner G, Blackler GM, Baatout S, Luxen A, et al. (2016) Improved aptamers for the diagnosis and potential treatment of HER2-positive cancer. Pharmaceuticals 29.
25. Fridman R, Benton G, Aranoutova I, Kleinman HK (2012) Increased initiation and growth of tumor cell lines, cancer stem cells and biopsy material in mice using basement membrane matrix protein (Cultrex or Matrigel) co-injection. Nat Protoc 6: 1138-1144.
26. Gijs M (2016) 68Ga-NOTA-oligonucleotides: applications for molecular PET imaging of HER2-positive cancer. J Labelled Comp Radiopharm 2: 63-71.
27. Deleye S, Verhaeghe J, Wyfells L, Dedeurwaerdere S, Stroobants S, et al. (2014) Towards a reproducible protocol for repetitive and semi-quantitative rat brain imaging with (18) F-FDG: exemplified in a memantine pharmacological challenge. Neuroimage 96: 276-287.
28. Fueger BJ, Czernin J, Hildebrandt I, Tran C, Halpern BS, et al. (2006) Impact of animal handling on the results of 18F-FDG PET studies in mice. J Nucl Med 6: 999-1006.
29. White RR, Sullenger BA, Rusconi CP (2000) Developing aptamers into therapeutics. J Clin Invest 8: 929-934.
30. Williams SV (2010) The SHrN™ scid hairless NOD mouse model: Development and characterization. Cancer Research 8: 393.
31. Wildt S (2013) Hairless NOD scid mouse, US20130205417 A1, Google Patents.
32. Cho HM, Rosenblatt J, Kang YS, Morrison AL, Penichet ML, et al. (2005) Enhanced inhibition of murine tumor and human breast tumor xenografts using targeted delivery of an antibody-endostatin fusion protein. Mol Cancer Ther 6: 956-967.
33. Sun M, Shi H, Liu C, Liu X, Liu J, et al. (2014) Construction and evaluation of a novel humanized HER2-specific chimeric receptor. Breast Cancer Res 3: 61.
34. Bandekar A, Kavre S, Chang MY, Mu Q, Rotolo J, et al. (2012) Antitumor efficacy following the intracellular and interstitial release of liposomal doxorubicin. Biomaterials 17: 4345-4352.
35. Healy J, Kewis SD, Kurz M, Boomer RM, Wilson C, et al. (2004) Pharmacokinetics and biodistribution of novel aptamer compositions. Pharm Res 21: 2234-2246.
36. Boomer RM, Lewis SD, Healy JM, Kurz M, Wilson C, et al. (2005) Conjugation to polyethylene glycol polymer promotes aptamer biodistribution to healthy and inflamed tissues. Oligonucleotides 3: 183-195.
37. Pardridge WM (2012) Drug transport across the blood-brain barrier. J Cereb Blood Flow Metab 11: 1959-1972.
38. D'Huyvetter M, Aerts A, Vaneycken I, Devooqdt N, Gijs M, et al. (2012) Development of 177Lu-nanobodies for radioimmunotherapy of HER2-positive breast cancer: evaluation of different bifunctional chelators. Contrast Media Mol Imaging 2: 254-264.
39. Price EW, Orvig C (2014) Matching chelators to radiometals for radiopharmaceuticals. Chem Soc Rev 1: 260-290.
40. Geselowitz DA, Neckers LM (1995) Bovine serum albumin is a major oligonucleotide-binding protein found on the surface of cultured cells. Antisense Res Dev 3: 213.
41. Tavitian B (2002) Oligonucleotides as radiopharmaceuticals. Molecular imaging. An essential tool in preclinical research, diagnostic imaging, and therapy. Springer, Germany.
42. Borkowski S, Dinkelborg L (2006) The Aptamer Handbook. Aptamers for In Vivo Imaging. Wiley, USA.
43. Yang F, Zhang Y, Liang H (2014) Interactive association of drugs binding to human serum albumin. Int J Mol Sci 3: 3580-3595.
44. Vallner JJ (1977) Binding of drugs by albumin and plasma protein. J Pharm Sci 4: 447-465.
45. Aspitia MA (2013) Soluble human epidermal growth factor receptor 2 (HER2) levels in patients with HER2-positive breast cancer receiving chemotherapy with or without trastuzumab: results from North Central Cancer Treatment Group adjuvant trial N9831. Cancer 15: 2675-2682.
46. Tse C, Gauchez AS, Jacot W, Lamy PJ (2012) HER2 shedding and serum HER2 extracellular domain: biology and clinical utility in breast cancer. Cancer Treat Rev 2: 133-142.
47. Pieve CD, Perkins AC, Missailidis S (2009) Anti-MUC1 aptamers: radiolabelling with (99m)Tc and biodistribution in MCF-7 tumour-bearing mice. Nucl Med Biol 6: 703-710.
48. Pieve CD, Blackshaw E, Missalidis E, Perkins AC (2012) PEGylation and biodistribution of an anti-MUC1 aptamer in MCF-7 tumor-bearing mice. Bioconjug Chem 7: 1377-1381.
49. Wu X, Liang H, Tan Y, Yuan C, Li S, et al. (2014) Cell-SELEX aptamer for highly specific radionuclide molecular imaging of glioblastoma in vivo. PLoS One 6: 90752.
50. Younes CK, Boisgard R, Tavitian B (2002) Labelled oligonucleotides as radiopharmaceuticals: pitfalls, problems and perspectives. Curr Pharm Des 16: 1451-1466.